7-2007

# Characterization of Hypereutectic Al-Si Powders Solidified under Far-From Equilibrium Conditions

Y. E. Kalay
*Iowa State University*

L. Scott Chumbley
*Iowa State University*, chumbley@iastate.edu

Iver E. Anderson
*Iowa State University*, andersoni@ameslab.gov

Ralph E. Napolitano
*Iowa State University*, ren1@iastate.edu

# Characterization of Hypereutectic Al-Si Powders Solidified under Far-From Equilibrium Conditions

**Abstract**
The rapid solidification microstructure of gas-atomized Al-Si powders of 15, 18, 25, and 50 wt pct Si were examined using scanning electron microscopy (SEM) and transmission electron microscopy (TEM). In order of increasing particle size, the powders exhibited microcellular Al, cellular/dendritic Al, eutectic Al, and primary Si growth morphologies. Interface velocity and undercooling were estimated from measured eutectic spacing based on the Trivedi–Magnin–Kurz (TMK) model, permitting a direct comparison with theoretical predictions of solidification morphology. Based on our observations, additional conditions for high-undercooling morphological transitions are proposed as an extension of coupled-zone predictions.

**Keywords**
Physical Chemistry

**Disciplines**
Metallurgy

**Comments**
This article is from *Metallurgical and Materials Transactions A* 38 (2007): 1452-1457, doi: 10.1007/s11661-007-9168-8. Posted with permission.

DOI: 10.1007/s11661-007-9168-8


# Characterization of Hypereutectic Al-Si Powders Solidified under Far-From Equilibrium Conditions

Y.E. KALAY, L.S. CHUMBLEY, I.E. ANDERSON, and R.E. NAPOLITANO

The rapid solidification microstructure of gas-atomized Al-Si powders of 15, 18, 25, and 50 wt pct Si were examined using scanning electron microscopy (SEM) and transmission electron microscopy (TEM). In order of increasing particle size, the powders exhibited microcellular Al, cellular/dendritic Al, eutectic Al, and primary Si growth morphologies. Interface velocity and undercooling were estimated from measured eutectic spacing based on the Trivedi–Magnin–Kurz (TMK) model, permitting a direct comparison with theoretical predictions of solidification morphology. Based on our observations, additional conditions for high-undercooling morphological transitions are proposed as an extension of coupled-zone predictions.

## I. INTRODUCTION

ATTRIBUTED primarily to its ability to achieve high cooling rates in a single process step for large quantities of material, gas atomization is, perhaps, the most industrially significant technique for rapid solidification, with over 50,000 tons of material produced by this method each year.[1] From a scientific standpoint, atomization methods provide experimental access to very high undercoolings in a containerless environment, presenting an opportunity to investigate the fundamentals of nucleation and growth in highly driven systems. In addition, the droplet size itself is a useful metric of the prevailing undercooling or cooling rate, and the atomization of a volume of liquid will typically produce a large range of droplet sizes, corresponding to a wide range of cooling rates. Thus, a quantity of atomized powder will exhibit a spectrum of solidification microstructures. Detracting from the scientific utility of the atomization method, however, is the chaotic nature of the process, which gives rise to considerable variation of microstructure, even for droplets of a particular size. Accordingly, employing gas atomization for the systematic study of solidification can be problematic.

Numerous atomization experiments for fundamental investigation of microstructural evolution during rapid solidification have been reported.[2,3,4] A detailed investigation of the correlation between undercooling and microstructure was performed by Levi and Mehrabian,[2] who used a vacuum-electrohydrodynamic atomization process to produce submicron powders of Al-Si and Al-Cu alloys. The typical microstructure exhibited by their powders revealed that solidification occurred primarily in two stages, beginning with the planar growth of a supersaturated solid solution followed by a transition to a cellular morphology and the concomitant segregation pattern. This two-stage freezing behavior has been observed by others[5] and indicates a transition from the rapid cooling associated with the absorption of latent heat by the droplet itself to the slower cooling associated with the transfer of heat to the particle's surroundings (*i.e.,* Newtonian cooling). Atomized particles often exhibit a clear microstructural transition associated with the change in cooling rate that accompanies the onset of Newtonian dominated cooling. Indeed, while microstructures were observed to vary within any given particle size range, the results of Levi and Mehrabian clearly indicate that decreasing particle size can be generally correlated with increasing undercooling and a departure from Newtonian cooling conditions. Thus, for smaller particles, solidification during recalescence becomes dominant and the transition to external heat-transfer control is suppressed. In the adiabatic limit, undercooling is sufficiently high that all of the latent heat liberated by the freezing droplet can be accommodated within the droplet itself and no external heat extraction is required for solidification. These general features have been well evidenced by microstructural observations,[2] where smaller particle sizes have been associated with an increasing degree of planar growth of the supersaturated solid solution and a suppression of the segregation-induced transition from planar to cellular growth morphologies.

In the current study, we employ high-pressure gas atomization to investigate microstructural selection in hypereutectic Al-Si alloys. In particular, we examine microstructural selection at high undercoolings and compare our observations with the selection map reported by Trivedi *et al.*[4] In addition, we consider the implications of our observations with respect to the onset of nonequilibrium solidification phenomena and non-Newtonian cooling conditions.

## II. EXPERIMENTAL PROCEDURE

Hypereutectic alloy powders of Al-15Si, Al-18Si, Al-25Si, and Al-50Si (wt pct) were produced using high-pressure gas atomization. For each experiment, the melt chamber of the gas atomizer was charged with high-purity (99.95 pct) Al and (99.99 pct) Si to a total weight of about 1.5 kg. Each charge was induction melted to 400 °C above the relevant liquidus temperature in a hard-fired bottom-pouring crucible made from high-purity (99.7 pct) $Al_2O_3$. Atomization was accomplished using ultrahigh purity (99.995 pct) nitrogen with a supply pressure of 6.6 MPa. The powder collected from each experiment was screened using ASTM standard vibratory sieves to obtain particles with diameters

Y.E. KALAY, Graduate Student, and L.S. CHUMBLEY, I.E. ANDERSON, and R.E. NAPOLITANO, Professors, are with Metal and Ceramic Sciences, Ames Laboratory, United States Department of Energy, and the Department of Materials Science and Engineering, Iowa State University, Ames, IA 50011. Contact e-mail: yekalay@iastate.edu

This article is based on a presentation made in the symposium entitled "Solidification Modeling and Microstructure Formation: In Honor of Prof. John Hunt," which occurred March 13–15, 2006, during the TMS Spring Meeting in San Antonio, Texas, under the auspices of the TMS Materials Processing and Manufacturing Division, Solidification Committee.

of ≤45 $\mu$m. Air classification and sedimentation methods were then used to isolate particles in size classes of 0 to 5 $\mu$m and 5 to 10 $\mu$m.

Samples selected for scanning electron microscopy (SEM) analysis were mounted in epoxy resin, ground, polished, and etched (in aqueous solution of 3 pct HCl, 2 pct $HNO_3$, and 1 pct HF, by volume) for cross-sectional analysis. In any given specimen, the largest particle cross sections were selected for examination to best ensure near-diametral sections. In addition, the particle diameter was measured on cross-sectional planes, which include at least three particles in contact, again ensuring a true diametral measurement. For transmission electron microscopy (TEM) investigation, selected powders were dispersed in epoxy, and the mixture was cured, thinned, and argon-ion milled (4 kV acceleration voltage and 20 deg incident angle) to perforation. For both SEM and TEM analyses, only the most spherical particles were considered for quantitative investigation because they are the ones that most likely solidified during free fall in the chamber.

The relative dominance of the different growth morphologies was measured as a function of powder size and composition using a linear-intercept analysis on selected powder cross sections. A total of 80 particles were examined, ranging from 0.5 to 45 $\mu$m in diameter and from 15 to 50 wt pct in Si content. For each particle, a total line length equal to 3 times the particle diameter was used for the analysis. Measurements of eutectic spacing were also performed using a line-intercept method, where the eutectic spacing was simply taken as the reciprocal of one-half the measured linear density of phase boundary intersections. A total of 21 particles, all with a composition of 18 wt pct Si but ranging from 2 to 45 $\mu$m in diameter, were used for this analysis.

## III. RESULTS

The range of morphologies observed in the powder samples includes primary silicon, eutectic, dendritic/cellular primary aluminum, and a microcellular aluminum structure. This is illustrated in Figure 1, showing the microstructure in ~25-$\mu$m-diameter powders over a range of compositions, and in Figure 2, showing the microstructure in 18 wt pct Si powders over a range of particle sizes. For the larger powders, growth morphology was easily ascertained using SEM analysis, but finer particles (*i.e.,* <5 $\mu$m diameter) required TEM imaging.

The influence of composition on growth morphology is summarized in Figure 1 for large (~25 $\mu$m) diameter powders. These exhibit dominant morphologies of primary Si (Figure 1(a)), eutectic (Figure 1(b)), or primary aluminum (Figure 1(d)), for compositions of 50, 25, and 15 wt pct Si, respectively. Similarly, the morphology varies with particle size, as shown in Figure 2, for powders of 18 wt pct Si. Here, the dominant morphology varies from eutectic at 30 $\mu$m (diameter) to cellular plus eutectic at 20 $\mu$m, cellular at 4 to 10 $\mu$m, and microcellular at 0.4 $\mu$m. For our purposes, we differentiate the microcellular morphology from the cellular morphology on the basis of the intercellular structure. Thus, the cellular structure contains a resolvable two-phase intercellular constituent (Figure 2(d)), where the microcellular morphology exhibits a distinguishable cellular segregation pattern, but no clearly distinguishable two-phase intercellular microstructure (Figure 2(f)). Rather, selected area diffraction reveals nanocrystalline Si and Al in the intercellular region.

The relative amount of each type of microstructure measured for two powder size classes (2 to 4 $\mu$m and 20 to 24 $\mu$m diameter) is plotted in Figure 3 as a function of alloy composition. This figure shows that, for the 20- to 24-$\mu$m size class, as the alloy composition is decreased from 50 wt pct Si to 18 wt pct Si, the dominant microstructure shifts from primary silicon to a eutectic morphology. The interpolated curves suggest that such a transition occurs at approximately 41 $\mu$m. As expected, further decrease in silicon content to 15 wt pct results in an increase in primary dendritic aluminum, although the eutectic structure remains as the majority constituent. In the 2- to 4-$\mu$m size class, the aluminum microcellular morphology is dominant at all compositions. Primary silicon is the prevalent secondary structure for alloys with 25 wt pct Si or higher, but the amount drops rapidly for lower Si content, as the eutectic constituent emerges. This size class is further characterized by growth morphologies that indicate free-surface nucleation, owing to the limited availability of bulk nucleation sites in very fine particles.

As a means for the estimation of undercooling, powders of 18 wt pct silicon, which were generally observed to be dominated by the eutectic morphology, were selected for the measurement of eutectic spacing. The results are shown in Figure 4, where measured eutectic spacings are plotted as a function of powder diameter and are compared with results from a previous study,[6] where helium, rather than nitrogen, was used as the atomizing gas.

## IV. DISCUSSION

The variation of eutectic spacing with particle diameter, plotted in Figure 4, indicates that the atomization gas has a measurable effect on undercooling for large particles. This is not particularly surprising, given that the heat capacity and thermal conductivity for helium gas are much greater than those for nitrogen gas. The plot indicates, however, that for particles less than ~10 $\mu$m, the undercooling may not be measurably dependent on these factors, perhaps indicating the threshold diameter below which the solidification rate is primarily governed by the heat absorption that occurs during recalescence, as discussed by Mehrabian *et al.*[2,3]

The values of undercooling ($\Delta T$) and interface velocity ($v$), corresponding to the various particle sizes, are plotted in Figures 5(a) and (b). These values were obtained from the eutectic spacing ($\lambda$) measurements for the 18 wt pct alloy, using the Trivedi–Magnin–Kurz (TMK) model[7] for eutectic growth at high velocity, and are based on the equations

$$\Delta T = \frac{ma^L}{\lambda}(1+q) \quad [1]$$

$$v = \frac{a^L q}{\lambda^2 Q^L} \quad [2]$$

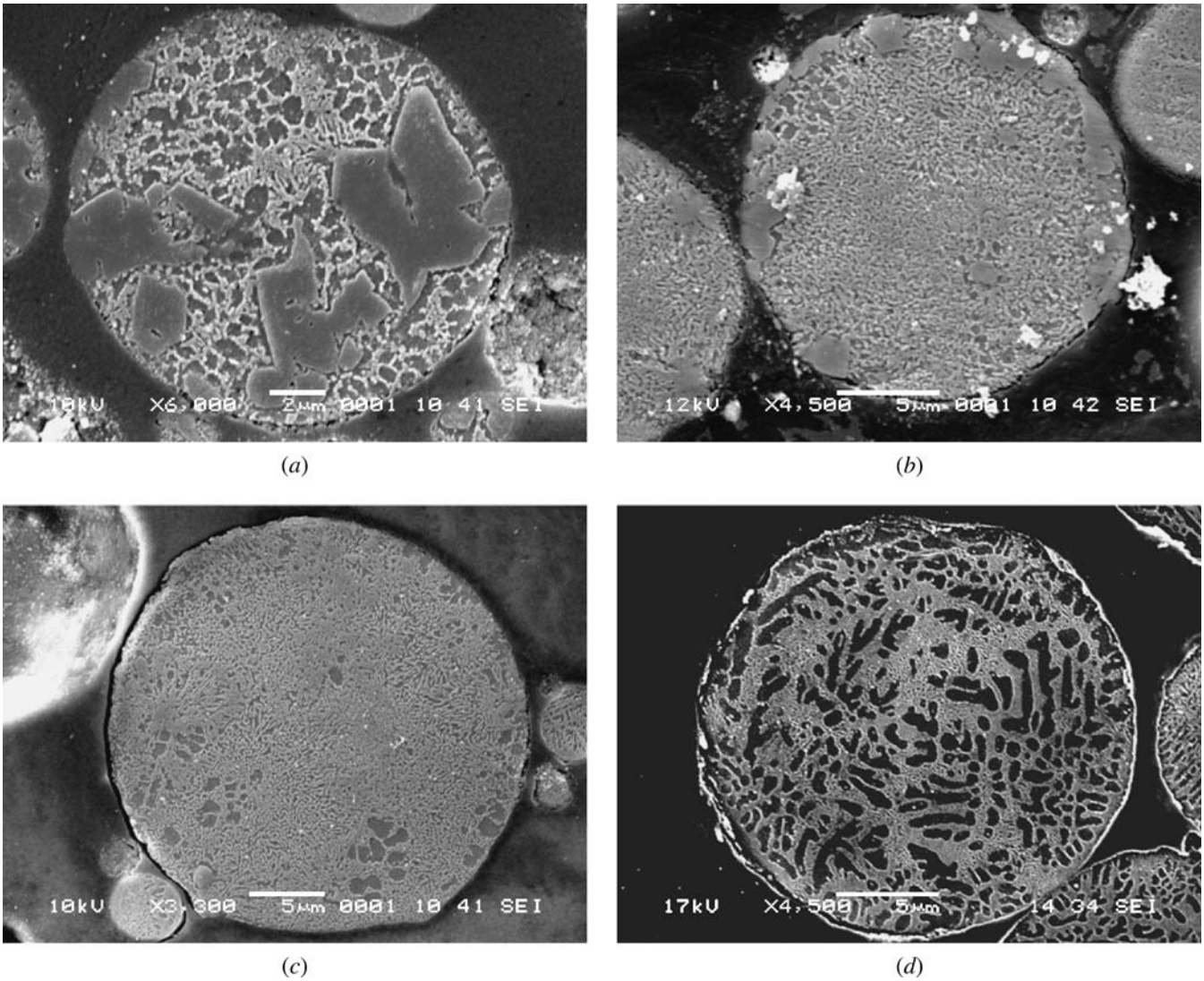


(*a*) (*b*) (*c*) (*d*)

Fig. 1—Representative microstructures of rapidly solidified powders (~25-$\mu$m diameter): (*a*) Al-50 wt pct Si, showing faceted primary Si, eutectic, and dendritic structures; (*b*) Al-25 wt pct Si, showing a large amount of eutectic; (*c*) Al-18 wt pct Si, showing primary Al and eutectic; and (*d*) 15 wt pct Si,[6] showing primary Al and eutectic.

where $m$, $a^L$, and $Q^L$ are defined by Eq. [16] in Reference 8, $q$ is defined here as

$$q \equiv \frac{P}{P + \lambda\left(\frac{\partial P}{\partial \lambda}\right)} \qquad [3]$$

and $P$ is a function of phase fraction, solute partition coefficient, and Peclet number, as described in Reference 7. Note that the value of $P$ approaches a constant for low Peclet numbers ($\lambda v/2D$), and $q$ approaches unity, where Eqs. [1] and [2] reduce to the Jackson–Hunt (JH) equations, $\lambda \Delta T = 2\, ma^L$ and $\lambda^2 v = a^L/Q^L$.[7] The material parameters used for the undercooling and velocity estimates are given in Table I.

For the low Peclet number (*i.e.,* $p < 0.2$) regime, corresponding to $d > 10$ $\mu$m and $v > 20$ mm/s, the JH and TMK models are in good agreement (Figure 6). Above this velocity (smaller particle diameter and higher Peclet number), there is a substantial difference between the models, indicating that nonequilibrium partitioning and temperature-dependent diffusivity are important considerations. Figure 5(c) shows that this $d > 10$ $\mu$m threshold corresponds to a Peclet number of approximately 0.2. It is interesting to note that this threshold in the Peclet number, where rapid solidification effects become important, coincides with the observed transition to recalescence-controlled growth rate, indicated by Figure 4.

Given the estimated undercooling values of Figure 5(b), the implications of the observed microstructure measurements can be considered in light of the morphology selection map previously proposed by Trivedi *et al*.[4] This map, along with the current experimental observations, is shown in Figure 7. The dashed vertical lines indicate the alloy compositions used for this study, and each symbol represents the indicated microstructural observation. It should be noted that these data indicate the *dominant* microstructure and do not imply that only a single morphology was observed. It should also be recognized that the analytical

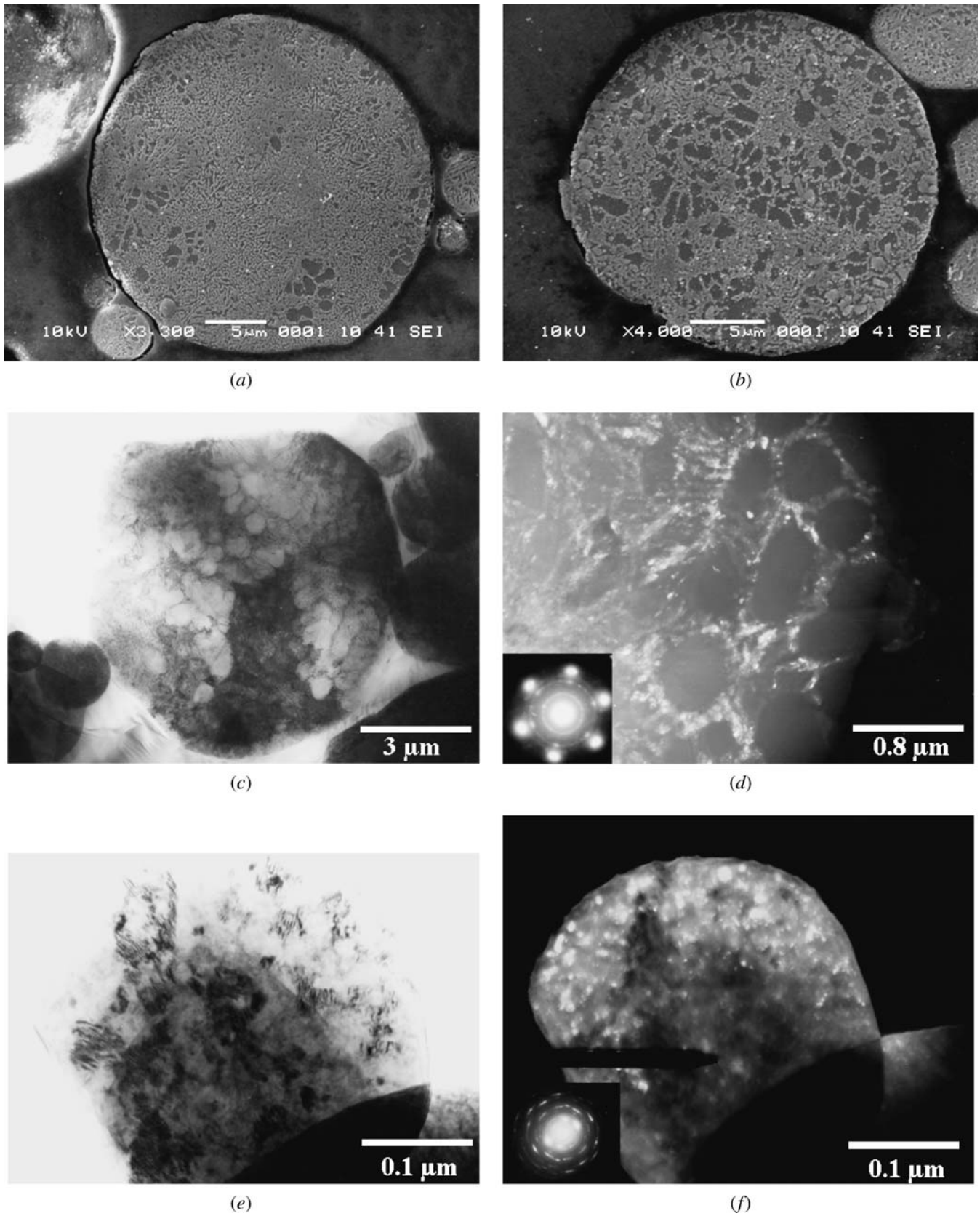


Fig. 2—Al-18 wt pct Si microstructures in powder particles of various diameter: (*a*) 30 $\mu$m, (*b*) 20 $\mu$m, (*c*) 10 $\mu$m, (*d*) 4 $\mu$m, and (*e*) and (*f*) 0.4 $\mu$m. Imaging: (*a*) and (*b*) secondary electron SEM, (*c*) and (*e*) bright-field TEM, and (*d*) and (*f*) dark-field TEM.

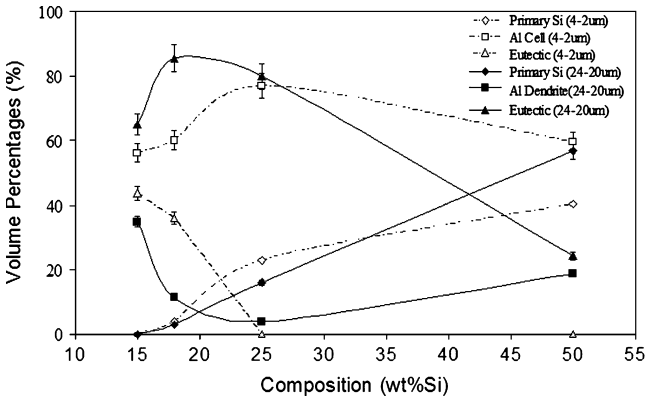


Fig. 3—The relative amount of each observed microstructure type, as a function of composition and powder size.

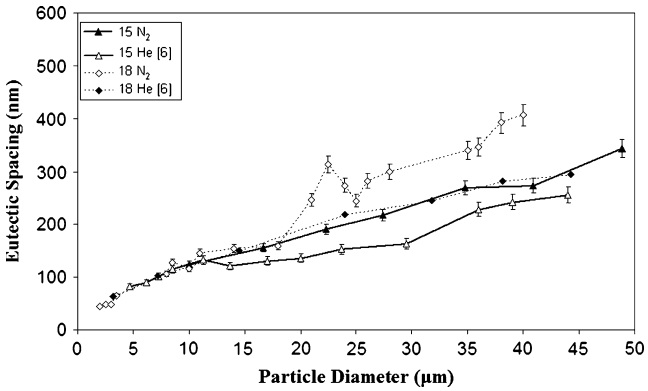


Fig. 4—Measured eutectic spacing *vs* powder diameter in 18 wt pct Si compared to results from Ref. 6.

predictions shown[4] indicate transitions in the favored growth morphology, where boundaries are defined by equal velocity at the given temperature. Such a calculation does not include any consideration of the time scale of competition dynamics and is not meant to imply that a single morphology would be observed in the microstructure. Rather, it is expected that several competing morphologies would be observed under many conditions. Finally, we point out that the prediction does not include any consideration of nucleation phenomena, which may play an important role in overall selection dynamics.

Focusing on the predicted transitions in growth morphology, observed microstructures are in good agreement with previously calculated microstructure regions. For example, the largest size particles of all compositions show primary Si formation being dominant. As particle size decreases, eutectic growth morphology becomes dominant for all compositions, although this transition occurs at a Si content that decreases with increasing powder diameter. Thus, the eutectic morphology is seen in powders of diameter 40 $\mu$m for 15 wt pct Si, 30 $\mu$m for 18 wt pct, and 25 $\mu$m for 25 wt pct, corresponding to temperatures of 840, 810, and 780 K respectively, in good agreement with the map. Examination of the 50 wt pct Si powders shows that the primary Si region extends to powders of size >3 to 4 $\mu$m, at which point the microcellular structure becomes dominant. Similarly, the calculated transition from eutectic to primary Al growth at low Si compositions and smaller powder sizes is also well supported by experimental observations, being seen in 15, 18, and 25 wt pct alloys.

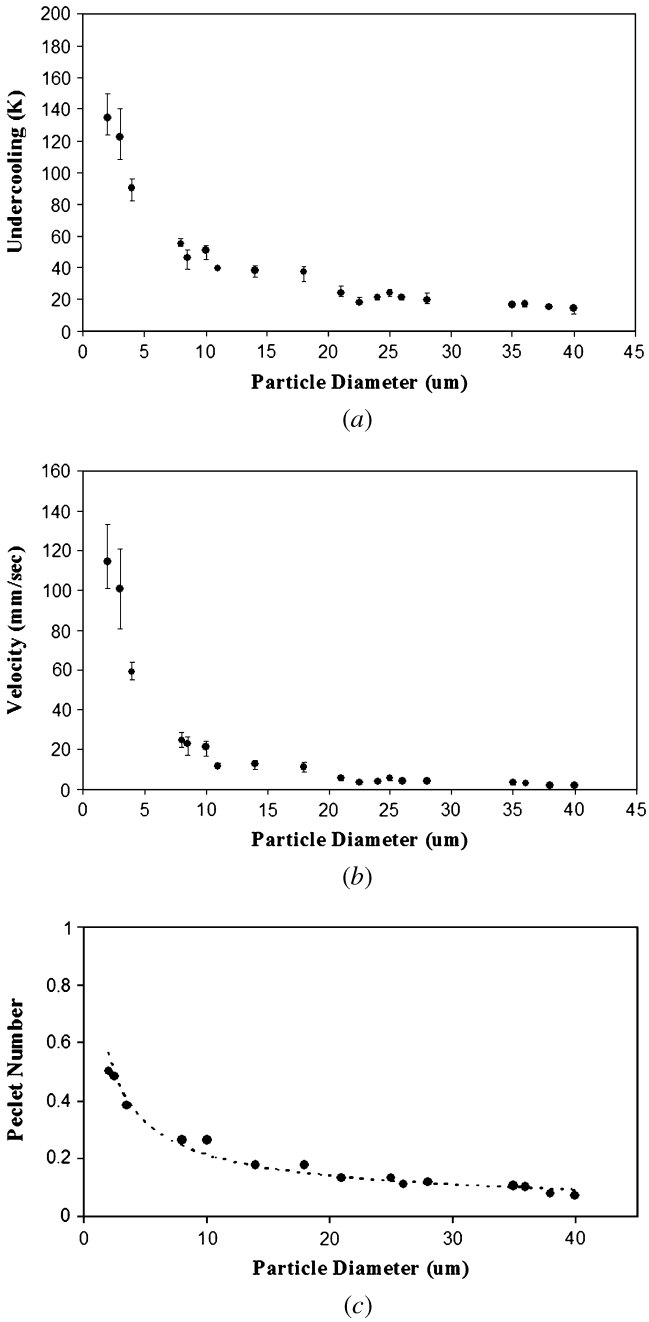


Fig. 5—(*a*) Growth velocity, (*b*) undercooling, and (*c*) Peclet number for eutectic growth, all estimated from eutectic spacing measurements in the 18 wt pct Si powders.

In powders dominated by primary Al formation, a fairly continuous transition appears from dendritic to cellular to microcellular. The transition from cellular, where clearly identifiable lamellar eutectic formation is observable, to the refined microcellular structure begins approximately at a powder diameter of 10 $\mu$m ($p \approx 0.2$) for 15 to 25 wt pct Si alloys. While no sharp morphological transition was observed in

**Table I. Parameters used in Undercooling and Velocity Estimates**

| Parameter Symbol | Parameter Value | Unit | Parameter Name |
|---|---|---|---|
| $D$ | $5 \times 10^{-9}$ | $m^2/s$ | diffusion coefficient |
| $C$ | 98.2 | wt pct | length of eutectic tie-line |
| $m_\alpha$ | 7.5 | K/wt pct | $\alpha$-phase liquidus slope |
| $m_\beta$ | 17.5 | K/wt pct | $\beta$-phase liquidus slope |
| $\Gamma_\alpha$ | $1.96 \times 10^{-7}$ | Km | Gibbs–Thomson coefficient ($\alpha$ phase) |
| $\Gamma_\beta$ | $1.7 \times 10^{-7}$ | Km | Gibbs–Thomson coefficient ($\beta$ phase) |
| $\theta_\alpha$ | 30 deg<br>0.524 | deg<br>rads | angle of $\alpha$ phase |
| $\theta_\beta$ | 65 deg<br>1.134 | deg<br>rads | angle of $\beta$ phase |
| $T_{eut}$ | 577.2 | °C | eutectic temperature |
| $C_{eut}$ | 0.126 | — | eutectic composition |
| $\rho_\alpha$ | $2.50 \times 10^6$ | g/m3 | density($\alpha$ phase) |
| $\rho_\beta$ | $2.33 \times 10^6$ | g/m3 | density($\beta$ phase) |
| $\Phi$ | 3.2 | — | extremum condition parameter[9] |

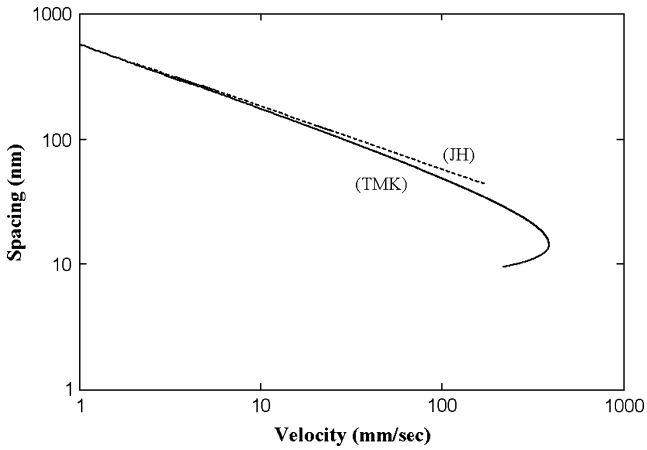


Fig. 6—The spacing-velocity relationship predicted by JH and TMK eutectic growth models for Al-18 wt pct Si, computed using the parameters in Table I.

any single particle, the existence of the microcellular structure shows a reasonable correlation with the convergent region in Figure 4, where recalescence appears to be controlling the growth rate. As we have noted, this transition is observed at a Peclet number that is coincident with the divergence of the TMK and JH models.

## V. CONCLUSIONS

Eutectic spacing measurements indicate that, for particle diameters less than 10 $\mu$m, the solidification rate may be unaffected by the type of gas used during atomization, suggesting that growth rate is governed by recalescence in this regime. Moreover, this diameter is consistent with the appearance of the microcellular growth morphology and with the divergence of the JH and TMK models for eutectic growth at Peclet numbers greater than ~0.2.

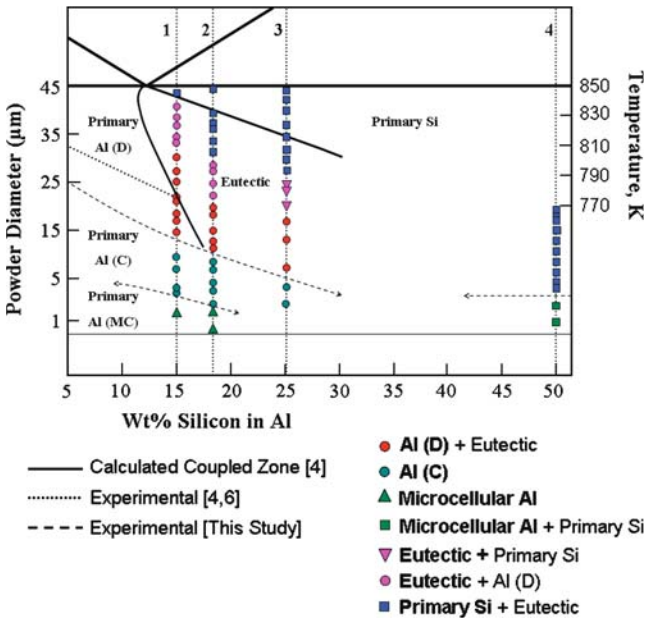


Fig. 7—Microstructure map[10] for the Al-Si system extended from the previously calculated map.[4] Lines 1 through 4 correspond to undercooling paths for Al-15 wt pct to 50 wt pct Si droplets.

Microstructure observations of large powders for alloys in the composition range from 15 to 50 wt pct Si agree well with the microstructure map proposed by Trivedi *et al.*[4]

The SEM and TEM observations of 18 wt pct Si indicate a continuous dendritic-cellular-microcellular transition that occurs with decreasing particle size. While the lamellar eutectic structure is easily discernable at large and midrange powder sizes, the intercellular constituents of the smallest size powders appear to consist of a nanocrystalline mixture of Si and Al.

## ACKNOWLEDMENTS

Appreciation is expressed to R. Trivedi for valuable discussions and his comments. This work was supported by the United States Department of Energy, Office of Basic Energy Sciences, Contract No. W-7405-ENG-82.

## REFERENCES

1. H. Jones: *Non Equilibrium Processing of Materials,* 1st ed., C. Suryanarayana, ed., Elsevier Science Ltd., Amsterdam, The Netherlands, 1999, pp. 23-45.
2. C.G. Levi and R. Mehrabian: *Metall. Trans. A,* 1982, vol. 13, pp. 13-23.
3. C.G. Levi and R. Mehrabian: *Metall. Trans. A,* 1982, vol. 13, pp. 221-34.
4. R. Trivedi, F. Jin, and I.E. Anderson: *Acta Mater.*, 2003, vol. 51, pp. 289-300.
5. L.A. Bendersky, F.S. Biancaniello, S.D. Ridder, and A.J. Shapiro: *Mater. Sci. Eng., A*, 1991, vol. 134, pp. 1098-102.
6. A.L. Genau: Master's Thesis, Iowa State University, Ames, IA, 2004.
7. R. Trivedi, P. Magnin, and W. Kurz: *Acta Metall.*, 1986, vol. 35, pp. 971-80.
8. K.A. Jackson and J.D. Hunt: *Trans. TMS-AIME*, 1966, vol. 236, pp. 1129-42.
9. H. Jones and W. Kurz: *Z. Metallkd.*, 1981, vol. 72, p. 792.
10. Y.E. Kalay, I.E. Anderson, L.S. Chumbley: International Conference on Powder Metallurgy and Particulate, *MPIF/AIME*, June 18-21, San Diego, CA, 2006, pp. 95-105.